Localization Dynamics of Fluids in Random Confinement

Thomas O. E. Skinner,[1] Simon K. Schnyder,[2] Dirk G. A. L. Aarts,[1] Jürgen Horbach,[2,*] and Roel P. A. Dullens[1,†]

[1]*Department of Chemistry, Physical and Theoretical Chemistry Laboratory, University of Oxford, South Parks Road, Oxford OX1 3QZ, United Kingdom*

[2]*Institut für Theoretische Physik II, Heinrich-Heine-Universität Düsseldorf, Universitätsstraße 1, 40225 Düsseldorf, Germany*

(Received 13 February 2013; published 17 September 2013)

The dynamics of two-dimensional fluids confined within a random matrix of obstacles is investigated using both colloidal model experiments and molecular dynamics simulations. By varying fluid and matrix area fractions in the experiment, we find delocalized tracer particle dynamics at small matrix area fractions and localized motion of the tracers at high matrix area fractions. In the delocalized region, the dynamics is subdiffusive at intermediate times, and diffusive at long times, while in the localized regime, trapping in finite pockets of the matrix is observed. These observations are found to agree with the simulation of an ideal gas confined in a weakly correlated matrix. Our results show that Lorentz gas systems with soft interactions are exhibiting a smoothening of the critical dynamics and consequently a rounded delocalization-to-localization transition.

DOI: 10.1103/PhysRevLett.111.128301 PACS numbers: 82.70.Dd, 61.43.−j, 64.60.Ht, 66.30.H−

Introduction.—Understanding the dynamics in disordered heterogeneous media is of great interest for fields like materials science, geophysics, or biology [1–3]. The mass transport in such media is associated with a strong separation of time scales, i.e., mobile particles that move through a ''matrix of immobile'' particles. Experimental realizations of such systems are binary mixtures of colloids with disparate sizes [4,5], ion-conducting glasses [6–10], or biological systems like cells [3].

To model such heterogeneous systems, one often treats the matrix particles as fixed. One of the simplest models is the disordered Lorentz gas [11,12] where a tracer particle moves in a matrix of fixed, randomly distributed, overlapping hard spheres. This model exhibits a delocalization-to-localization transition associated with the critical percolation point [13] of the void space. At low matrix densities, the void space is a percolating network leading to diffusive tracer motion, but it becomes disconnected above the critical percolation density, and the tracer is trapped in finite pockets of void space. At the critical point, the long-time diffusion is anomalous [14–16], characterized by a sublinear dependence of the mean squared displacement (MSD) on time, $\delta r^2(t) \sim t^x$ with $x \approx 2/3.036$ in two dimensions (2D) [16] and $x \approx 0.32$ in 3D [15].

It is an open question as to whether the Lorentz gas scenario is also relevant in complex media such as ion conductors or porous materials. Simulations have reported anomalous diffusion and localization dynamics in various more realistic heterogeneous systems such as binary mixtures with a frozen-in component [17–22] or a disparate size ratio [23] and realistic models of ion-conducting alkali silicate glasses [8]. These studies are corroborated by mode coupling theory calculations [24], which provide a qualitative description of the Lorentz gas [25] and predict localization transitions for disparate-sized binary mixtures [26] and quenched-annealed systems [27–30].

While models like the Lorentz gas are insightful, experimental realizations of systems with fixed, randomly placed matrix particles are very rare. Most experimental studies of diffusion in disordered media have been reported for porous glasses [31] where systematically varying the pore size distribution is very difficult. In this Letter, we present a 2D colloidal model experiment consisting of small tracer particles in a random confining matrix of fixed large particles. The experimental setup enables *in situ* control of the area fractions of the fluid and matrix particles *without* changing the matrix configuration, which is crucial for studying the localization dynamics in random media. The experiment exhibits delocalized tracer dynamics at low matrix area fractions and highly localized tracer motion at high matrix area fractions. Our experimental findings are supported by molecular dynamics (MD) simulations of a 2D soft sphere binary mixture with the large species being fixed and the small species forming an ideal fluid of noninteracting particles. The simulations indicate that the experimental localization transition is rounded due to the soft interactions, which lead to a distribution of energies of the tracers and finite barriers in the matrix. This is qualitatively different from the sharp localization transition in the Lorentz gas.

Experiment.—A mixture of 3.9 and 4.95 μm diameter superparamagnetic colloidal polystyrene spheres (Microparticles GmbH) in water is confined between two glass slides to make a 2D sample cell [Fig. 1(a)]. The large particles act as spacers and hence form the fixed matrix in which the small particles—the fluid—are free to move [32]. Video microscopy is used to image an area of 430 μm × 340 μm for up to 2 h. Standard tracking routines are used to find the matrix and fluid particle

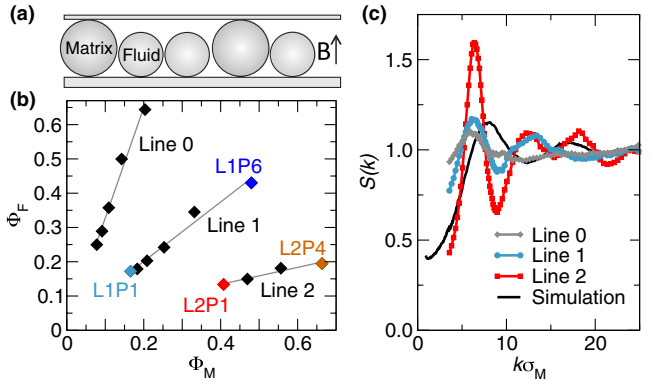

FIG. 1 (color online). (a) The sample cell with the matrix particles acting as spacers. (b) State diagram for the effective area fractions of the fluid (Φ_F) versus the matrix particles (Φ_M). (c) Structure factors of the matrix configurations for lines 0, 1, and 2 and the simulation.

coordinates [33] as a function of time from which we computed the static and dynamics quantities of interest.

In the experiments, we prepared three different samples which are represented by the three lines denoted line 0, 1, and 2 in the state diagram in Fig. 1(b). Each line, i.e., sample, corresponds to a different matrix configuration, and the lowest state point along each line is characterized by the hard sphere area fractions of the matrix (Φ_M^0) and the fluid (Φ_F^0) particles and is thus achieved without the presence of a magnetic field. The lowest state point of each line is labeled as "L1P1" for line 1, for example. To achieve higher *effective* packing fractions $\Phi_{F,M}$, we apply a perpendicular external magnetic field B which leads to a repulsive pair potential given by $U_{F,M}(r) = \mu_0 \chi_{F,M}^2 B^2/(4\pi r^3)$. Here, r is the distance between two particles, μ_0 the permeability of free space, and $\chi_{F,M}$ the magnetic susceptibility of the fluid or matrix particles. The state points with the magnetic field present are, e.g., "L1P2, ..., L1P6" for line 1. To represent these state points in the (Φ_M, Φ_F) state diagram, we calculate the effective hard sphere diameters $\sigma_{F,M}$ using a Barker-Henderson approach: $\sigma_{F,M} = \sigma_{F,M}^0 + \int_{\sigma_{F,M}^0}^{\infty} (1 - e^{-\beta U_{F,M}(r)}) dr$, where $\sigma_{F,M}^0$ are the hard sphere diameters and $\beta = 1/k_B T$ [34,35]. If $B = 0$, $\sigma_{F,M}$ reduces to $\sigma_{F,M}^0$, which corresponds to the lowest state point along each line. Note that the effective matrix to fluid particle size ratio remains fairly constant at 0.787, as is evident from the linear paths in the (Φ_F, Φ_M) state diagram [Fig. 1(b)].

The key point of our approach is that we *in situ* control the effective area fractions without changing the matrix configuration, so that we can very efficiently probe the tracer dynamics at different effective matrix and fluid area fractions. Importantly, we retain the random character of the matrix even at very high effective area fractions, which is crucial for studying the localization dynamics in random media and comparing it to the Lorentz gas. In our analysis of the tracer dynamics, we will focus on the state points along lines 1 and 2. The experimental data are averaged over up to five independent matrix configurations by imaging different parts of each sample.

First, we characterize the structural correlations of the matrix by computing its static structure factor $S(k) = \frac{1}{N_M} \langle \sum_{i=1}^{N_M} \sum_{j=1}^{N_M} e^{-i\vec{k}\cdot(\vec{r}_i - \vec{r}_j)} \rangle$. Here, N_M is the number of matrix particles, the angled brackets represent an ensemble average, and $\vec{r}_i$ and $\vec{r}_j$ are the positions of matrix particles i and j, respectively. The matrix structure factors corresponding to lines 0, 1, and 2 only show weak fluidlike structural correlation [Fig. 1(c)], similar to the uncorrelated Lorentz model. Note that the structure factors do *not* change along each line, which is a direct consequence of increasing the effective area fractions by increasing B. Importantly, it also directly confirms that the matrix particles are fixed.

We analyze the fluid particle dynamics by computing the mean squared displacement $\delta r^2(t) = \frac{1}{N_F} \langle \sum_{i=1}^{N_F} [\vec{r}_i(t) - \vec{r}_i(0)]^2 \rangle$, with N_F the number of fluid particles and $\vec{r}_i$ the position of fluid particle i. The MSDs along lines 1 and 2 are shown in Fig. 2(a). Note that the difference in the short-time diffusion is due to the different number densities [36,37] and that diffusion is well defined in 2D systems with fixed obstacles [16]. At L1P1, characterized by low matrix and low fluid area fractions, the tracer dynamics is diffusive at long times. Upon increasing the effective area fractions Φ_F and Φ_M along line 1, the dynamics shows a noticeable slowing down and strongly subdiffusive behavior at intermediate times. However, at long times, the MSDs of all the state points along line 1 exhibit diffusive behavior, corresponding to delocalized motion. Consistently, delocalized motion is observed at all state points along line 0, i.e., at lower matrix area fractions (data not shown). In contrast, the fluid particle dynamics exhibits completely different behavior along line 2, i.e., at much higher matrix area fractions. At L2P1, the MSD plateaus at long times, which upon increasing Φ_F and Φ_M along line 2, decreases to smaller values. This behavior clearly indicates the localization of the tracers in this region of the state diagram and shows that the length scale associated with the localization becomes smaller as the matrix area fraction is increased.

Simulation.—To gain more insight into the mechanism of the experimentally observed localized tracer dynamics, we perform detailed MD simulations of a quenched-annealed system: a binary system of purely repulsive soft spheres with the Weeks-Chandler-Andersen interaction potential [38], where the matrix particles are fixed. In particular, we simulate the tracer dynamics in the limit of $\Phi_F \to 0$, while we systematically increase the matrix area fraction, which enables us to efficiently sample the regions corresponding to both delocalized and localized tracer dynamics. Importantly, we do not aim to achieve

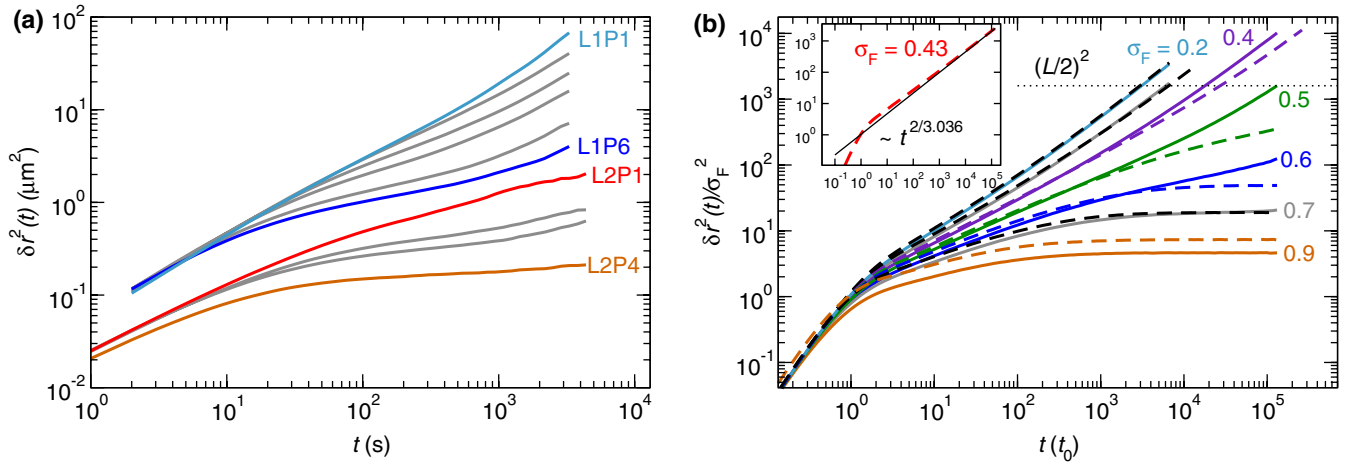

FIG. 2 (color online). (a) MSD for the fluid particles in the experiments along lines 1 and 2. (b) MSD for the fluid particles in the simulation for $\sigma_F = 0.2$, 0.3, 0.4, 0.5, 0.6, 0.7, and 0.9 for monoenergetic tracers (dashed lines) and tracers with a distribution of energies (solid lines). The dotted line roughly marks the limit above which finite size effects become important (with simulation box size L). Inset: Comparison of the MSD of the monoenergetic system at $\sigma_F = 0.43$ to the expected critical asymptote of the two-dimensional Lorentz model.

quantitative agreement between the experiments and the simulations. This is prohibitively difficult as—among other things—one would have to include hydrodynamic interactions and account for the change of the softness of the potential with the magnetic field. Instead, we feel that it is far more instructive to perform simulations with a different soft interaction potential and hence reveal generic features of the localization dynamics in Lorentz gas systems with soft interactions.

The parameters of the system and the MD simulation are set as in Ref. [23], except that the tracer interaction is turned off to avoid the effect of fluid-fluid interaction on the dynamics. The matrix particle diameters are sampled equidistantly $\sigma_M \in [0.85, 1.15]$ to avoid crystallization. For each realization of the system, between 1000 and 4000 matrix particles are equilibrated at number density $\rho = 0.278\sigma_M^{-2}$ at the temperature $k_BT = 1$ by randomly selecting their velocities from the Maxwell distribution every 100 steps, for 10^5 time steps. Then, the matrix particles are fixed and their positions are uniformly rescaled to $\rho = 0.625\sigma_M^{-2}$. The computed quantities are averaged over 100 independent matrix configurations. To simulate the tracer dynamics, we insert up to 1000 noninteracting fluid particles into each matrix configuration. We vary the tracer diameter σ_F, which is equivalent to varying the matrix area fraction without changing the structure of the matrix, analogous to the experiments. Varying the system size L allows us to control finite size effects, which only start to play a role after the MSD exceeds $\approx (L/2)^2$, as indicated in Fig. 2(b).

Comparison between simulation and experiment.—As in the experiments, the structure factor of the simulated matrix only shows weak fluidlike structural correlations [Fig. 1(c)]. In the simulations, we consider two cases: the tracers have either the *same* or a *distribution* of energies. In the first case, the tracers are given the same energy by first determining the average energy during equilibration and then re-inserting them such that the energy of each tracer equals the average energy. The simulations then reproduce the Lorentz model, as is evident from the MSD of the tracers for different values of σ_F [dashed lines in Fig. 2(b)]. In the long-time limit, the MSD changes from diffusive at small σ_F to localized at large σ_F with an extended subdiffusive regime at intermediate times. The localization-delocalization transition occurs approximately at $\sigma_F^* = 0.43$ (see the inset), where the MSD asymptotically approaches a power law $\delta r^2 \sim t^x$ with $x \approx 2/3.036$, in agreement with the Lorentz model [16].

The experimental system, however, is *not* an ensemble of tracers with the same energy but exhibits a broad distribution of tracer energies. Moreover, the barriers between the pores in the matrix are of finite height due to the soft interactions, which allows tracers with high energy to overcome barriers that cannot be surpassed by low-energy tracers. As a consequence, tracers with different energies have different critical points, which necessarily leads to an averaging of the dynamics: the localization transition is expected to be rounded, and hence the Lorentz model exponent cannot be measured in our experiments. To demonstrate this effect, we consider the second case and simulate a system where the tracers form an ideal gas, which is the simplest system of tracers with a distribution of energies. For comparison to the single-energy case, the average energy per tracer particle is kept the same. The ideal gas MSDs [solid lines in Fig. 2(b)] clearly differ from the single-energy case (dashed lines) at long times. The difference is most striking at $\sigma_F = 0.6$, where the single-energy system is clearly localized, while the ideal gas

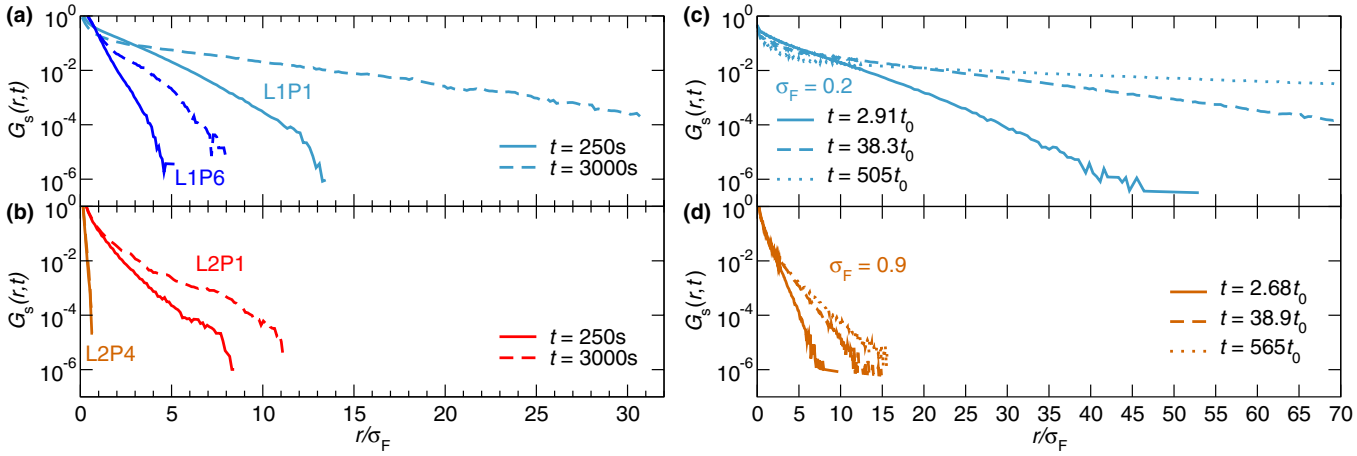

FIG. 3 (color online). (a) $G_s(r, t)$ for the fluid particles in the experiment along line 1 at state points 1 and 2 after 250 and 3000 s. (b) As in (a), but for line 2. (c) $G_s(r, t)$ for the fluid particles in the simulation for a delocalized state ($\sigma_F = 0.2$), (d) As in (c), but for a localized state ($\sigma_F = 0.9$).

system still shows diffusion at long times, as a substantial subset of the particles has high enough energies to be delocalized.

Our simulations thus show that Lorentz gas systems with soft interactions—as our experimental system—exhibit a rounded delocalization-to-localization transition. This can also be inferred from the experimental data in Fig. 2(a): the tracers at state point L1P6 are still diffusive at long times, while at state point L2P1, which has a comparable Φ_M but a far lower Φ_F, the tracers are localized. This is a direct consequence of the potential at high magnetic fields (L1P6) being much softer, which leads to a rounding of the localization transition, whereas L2P1 is characterized by a far harder potential and less rounding of the localization transition.

To further corroborate our findings, we also compute the self-part of the van Hove correlation function $G_s(r, t)$, as it gives the full spatial information for the tracer particle dynamics at a given time. This function gives the distribution of displacements $\Delta r_i = |\vec{r}_i(t) - \vec{r}_i(0)|$ of a tagged particle i at time t: $G_s(r,t) = \frac{1}{N_F}\langle\sum_{i=1}^{N_F}\delta(r - \Delta r_i)\rangle$ [39]. In Fig. 3(a), we show the experimental $G_s(r, t)$ for L1P1 and L1P6 at times $t = 250$ s and $t = 3000$ s. The lower time (250 s, solid lines) roughly corresponds to the time where subdiffusion is strongest, while the larger time (3000 s, dashed lines) marks the end of the experimental runs. The delocalized nature of the tracers at low area fractions is reflected by the broad distribution at L1P1 and its time dependence: the width increases by a factor of 3 from $t = 250$ s to $t = 3000$ s. At point L1P6, the shape of $G_s(r, t)$ is very similar compared to L1P1 but the distributions are narrower at both times, reflecting the much higher effective area fractions. The $G_s(r, t)$'s for L2P1 and L2P4 are shown in Fig. 3(b). Although the fluid particles at L2P1 are localized, which can only be inferred here from the time dependence, i.e., from the MSD, the $G_s(r, t)$ is fairly similar to that of L1P6—despite the fact that L2P1 is characterized by a far lower fluid area fraction. The very narrow $G_s(r, t)$ and the absence of any shift when changing from $t = 250$ s to $t = 3000$ s indicates a strong localization at L2P4.

In Figs. 3(c) and 3(d), we show $G_s(r, t)$ for the simulated confined ideal gas at three times, where the values of the MSD roughly agree with those of the experiment: $t \approx 3t_0$, $t \approx 39t_0$, and an additional time that is an order of magnitude larger $t \approx 550t_0$. The shape of $G_s(r, t)$ of the simulation at $\sigma_F = 0.2$ [Fig. 3(c)] matches the $G_s(r, t)$ of L1P1 [Fig. 3(a)] well. As σ_F increases, $G_s(r, t)$ in the simulation undergoes the same qualitative development as in the experiment. On the localized side [$\sigma_F = 0.9$, Fig. 3(d)], a very narrow distribution is observed that shows virtually no change with time, except from a small broadening which qualitatively matches the experimental data at L2P1 and L2P4. The general agreement between experiment and simulation also shows that fluid-fluid interactions are not important in the experiment. This is additionally indicated by the fact that there is no sign of particle hopping in the experimental $G_s(r, t)$ which would result in peaks or shoulders at distances comparable to the nearest-neighbor distance between two tracer particles [note that the quantity $2\pi r G_s(r, t)$ also does not show such a feature] [8,18].

Conclusion.—We have studied the localization dynamics of two-dimensional fluids confined in a random matrix using colloidal experiments and molecular dynamics simulations. In the experiments, mean squared displacements and van Hove correlation functions show signatures of delocalized tracer dynamics at low matrix area fractions and localized motion at high matrix area fractions. In particular, we observe long-time diffusion at small matrix area fractions, while trapping in finite pockets of the matrix is present at high matrix area fractions. The molecular dynamics simulations show that the soft interactions in our colloidal model system, which give rise to an energy

distribution for the tracer particles, smoothen the critical dynamics and enhance the diffusivity, leading to a rounded localization transition. Our results show that the smoothening of the critical dynamics does not depend on the details of the interaction potential, which suggests that the rounding of the localization transition is a generic feature of realistic systems.

We thank Pinaki Chaudhuri for useful discussions. S. K. S. and J. H. acknowledge the DFG research unit FOR-1394 "Nonlinear response to probe vitrification" (HO 2231/7-1); T. O. E. S., D. G. A. L. A., and R. P. A. D. acknowledge the EPSRC; J. H. and R. P. A. D. acknowledge the Royal Society for financial support.

*horbach@thphy.uni-duesseldorf.de
†roel.dullens@chem.ox.ac.uk

[1] M. Sahimi, Rev. Mod. Phys. **65**, 1393 (1993).
[2] D. B. Dingwell, Science **273**, 1054 (1996).
[3] F. Höfling and T. Franosch, Rep. Prog. Phys. **76**, 046602 (2013).
[4] A. Imhof and J. K. G. Dhont, Phys. Rev. E **52**, 6344 (1995).
[5] A. Imhof and J. K. G. Dhont, Phys. Rev. Lett. **75**, 1662 (1995).
[6] A. K. Jonscher, Nature (London) **267**, 673 (1977).
[7] A. Bunde, K. Funke, and M. D. Ingram, Solid State Ionics **105**, 1 (1998).
[8] J. Horbach, W. Kob, and K. Binder, Phys. Rev. Lett. **88**, 125502 (2002).
[9] T. Voigtmann and J. Horbach, Europhys. Lett. **74**, 459 (2006).
[10] J. C. Dyre, P. Maass, B. Roling, and D. L. Sidebottom, Rep. Prog. Phys. **72**, 046501 (2009).
[11] H. A. Lorentz, Proc. R. Acad. Sci. Amsterdam **7**, 438 (1905).
[12] H. van Beijeren, Rev. Mod. Phys. **54**, 195 (1982).
[13] D. Stauffer and A. Aharony, *Introduction to Percolation Theory* (Taylor and Francis, London, 1991).
[14] D. Ben-Avraham and S. Havlin, *Diffusion and Reactions in Fractals and Disordered Systems* (Cambridge University Press, Cambridge, England, 2000).
[15] F. Höfling, T. Franosch, and E. Frey, Phys. Rev. Lett. **96**, 165901 (2006).
[16] T. Bauer, F. Höfling, T. Munk, E. Frey, and T. Franosch, Eur. Phys. J. Special Topics **189**, 103 (2010).
[17] J. Kurzidim, D. Coslovich, and G. Kahl, Phys. Rev. Lett. **103**, 138303 (2009).
[18] J. Kurzidim, D. Coslovich, and G. Kahl, Phys. Rev. E **82**, 041505 (2010).
[19] J. Kurzidim, D. Coslovich, and G. Kahl, J. Phys. Condens. Matter **23**, 234122 (2011).
[20] K. Kim, K. Miyazaki, and S. Saito, Europhys. Lett. **88**, 36 002 (2009).
[21] K. Kim, K. Miyazaki, and S. Saito, Eur. Phys. J. Special Topics **189**, 135 (2010).
[22] K. Kim, K. Miyazaki, and S. Saito, J. Phys. Condens. Matter **23**, 234123 (2011).
[23] T. Voigtmann and J. Horbach, Phys. Rev. Lett. **103**, 205901 (2009).
[24] W. Götze, *Complex Dynamics in Glass-Forming Liquids* (Oxford University Press, Oxford, England, 2009).
[25] M. Spanner, S. K. Schnyder, F. Höfling, T. Voigtmann, and T. Franosch, Soft Matter **9**, 1604 (2013).
[26] T. Voigtmann, Europhys. Lett. **96**, 36 006 (2011).
[27] V. Krakoviack, Phys. Rev. Lett. **94**, 065703 (2005).
[28] V. Krakoviack, Phys. Rev. E **75**, 031503 (2007).
[29] V. Krakoviack, Phys. Rev. E **79**, 061501 (2009).
[30] V. Krakoviack, Phys. Rev. E **84**, 050501 (2011).
[31] M. C. Bellissent-Funel, J. Lal, and L. Bosio, J. Chem. Phys. **98**, 4246 (1993).
[32] G. Cruz de León, J. M. Saucedo-Solorio, and J. L. Arauz-Lara, Phys. Rev. Lett. **81**, 1122 (1998).
[33] J. C. Crocker and D. G. Grier, J. Colloid Interface Sci. **179**, 298 (1996).
[34] J. A. Barker and D. Henderson, J. Chem. Phys. **47**, 4714 (1967).
[35] J. P. Hansen and I. R. McDonald, *Theory of Simple Liquids* (Academic, London, 2006).
[36] X. Qiu, X. L. Wu, J. Z. Xue, D. J. Pine, D. A. Weitz, and P. M. Chaikin, Phys. Rev. Lett. **65**, 516 (1990).
[37] Y. Peng, W. Chen, T. M. Fischer, D. A. Weitz, and P. Tong, J. Fluid Mech. **618**, 243 (2009).
[38] J. D. Weeks, D. Chandler, and H. C. Andersen, J. Chem. Phys. **54**, 5237 (1971).
[39] K. Binder and W. Kob, *Glassy Materials and Disordered Solids* (World Scientific, Singapore, 2011).